J. Fluid Mech. (1994), *vol.* 263, *pp.* 361–374

Entropy maximization tendency in topographic turbulence

By JIEPING ZOU AND GREG HOLLOWAY
Institute of Ocean Sciences, PO Box 6000, Sidney, BC V8L 4B2, Canada

(Received 5 January 1993 and in revised form 24 September 1993)

Numerical simulations of geostrophic turbulence above topography are used to compare (*a*) nonlinear generation of system entropy, S, (*b*) selective damping of enstrophy and (*c*) development of vorticity–topography correlation. In the damped cases, S initially increases, approaching a quasi-equilibrium (maximum S subject to the instantaneous, though decaying, energy and enstrophy). When strongly scale-selective damping is applied, onset of the vorticity–topography correlation follows the timescales for enstrophy decay. During the period of decay, it is shown that nonlinear interaction continues to generate S, offsetting in part the loss of S to explicit damping.

1. Introduction

H theorems for statistical fluid dynamics (Carnevale, Frisch & Salmon 1981, hereinafter referred to as CFS) have demonstrated entropy maximization tendency as an inherent property of non-dissipative second-order turbulence closure equations for a range of problems. The concept of entropy maximization may also be relevant for dissipative dynamics, in particular, for turbulence over irregular topography (Holloway 1978). This tendency has been demonstrated in relation to approach to absolute equilibrium (Carnevale 1982), predictability of fluid motions (Carnevale & Holloway 1982; Carnevale & Vallis 1984), and internal gravity wave dynamics (Frederiksen & Bell 1983, 1984). Implication of the tendency in two-dimensional atmospheric flows on a sphere has been examined by Frederiksen & Sawford (1980). The implication in ocean circulation on a β-plane basin has been considered in Salmon, Holloway & Hendershott (1976) (hereinafter referred to as SHH), Holloway (1986), Griffa & Salmon (1989) and Cummins (1992), identifying the tendency with emergence of Fofonoff gyres from initial random eddy fields. It has been argued that the tendency may serve as a means of parameterization for unresolved scales in coarse resolution ocean models (Holloway 1992).

The present paper examines how entropy maximization is manifested in numerical simulation of turbulence over irregular topography. Questions we address are: (i) how the entropy maximization proceeds in dissipative systems; and (ii) to what extent entropy serves as a diagnostic in relation to development of vorticity–topography correlation. Discussions are complemented with examination of the enstrophy minimization process (Bretherton & Haidvogel 1976). We recall statistical theories and make observations about qualitative behaviour of entropy (§2). We then present numerical results, including discussion of approximate entropy calculation for isotropic flow (§3), with remarks in §4.

2. Statistical theory

Consider a homogeneous, rotating layer of fluid over irregular topography. Given the smallness of Rossby number and fractional change in the layer thickness, the fluid motion is governed by the potential vorticity equation. In spectral form (Holloway 1978)

$$(\mathrm{d}/\mathrm{d}t)\,\zeta_k + \sum_{k+p+q=0} A_{kpq}(\zeta_{-p}\,\zeta_{-q} + \zeta_{-p}\,h_{-q}) = \nu_k\,\zeta_k, \tag{1}$$

where ζ_k and h_{-q} are Fourier modes in wavevectors $\boldsymbol{k}$ and $-\boldsymbol{q}$, respectively for vorticity and fractional height of topography (multiplied by Coriolis parameter). The summation, corresponding to the Jacobian term $J(\psi, \zeta+h)$ in physical space, is taken over all $\boldsymbol{p}$ and $\boldsymbol{q}$ modes for which $\boldsymbol{k}+\boldsymbol{p}+\boldsymbol{q}=\boldsymbol{0}$. ν_k is the spectral representation of dissipation operator to be specified as needed. $A_{kpq} = (p_x q_y - p_y q_x)/p^2$ is the interaction coefficient.

Numerical simulations (Bretherton & Haidvogel 1976) demonstrated that a realization of (1), starting from a random field uncorrelated with bottom topography, will quickly develop vorticity–topography correlation in a sense of clockwise circulation over 'bumps' and anti-clockwise over 'dips'. Equilibrium statistics of an ensemble of such realizations without force and dissipation can be determined from the canonical distribution $\mathscr{P}(\{\zeta_k\}) \propto \exp\{-\sigma E - \mu Q\}$ (SHH), where E energy and Q potential enstrophy are two quadratic invariants of (1),

$$E = \tfrac{1}{2}\sum_k |\zeta_k|^2/k^2 \quad \text{and} \quad Q = \tfrac{1}{2}\sum_k |\zeta_k + h_k|^2,$$

and σ, μ are Lagrange multipliers to be determined from prescribed $\langle E\rangle = E_0$ and $\langle Q\rangle = Q_0$, with $\langle\ \rangle$ denoting ensemble average. Statistical moments from the canonical distribution,

$$\langle \psi_k \rangle^{eq} = h_k/((\sigma/\mu)+k^2), \tag{2a}$$

$$\langle \zeta_{-k}\,\zeta_k \rangle^{eq} = 2k^2/(\sigma+\mu k^2) + \mu^2 k^4 \langle h_{-k}\,h_k\rangle/(\sigma+\mu k^2)^2, \tag{2b}$$

$$\langle \zeta_{-k}\,h_k \rangle^{eq} = -\mu k^2 \langle h_{-k}\,h_k\rangle/(\sigma+\mu k^2), \tag{2c}$$

exhibit strong correlation between flow and topography. Specifically, $\langle\psi_k\rangle^{eq} \propto h_k$ on large scale, $\langle\zeta_k\rangle^{eq} = -k^2\langle\psi_k\rangle \propto -h_k$ on small scales, and $\langle\zeta_{-k}\,\zeta_k\rangle^{eq}$ has a steady component proportional to $\langle h_{-k}\,h_k\rangle$. Non-equilibrium results from closure equations exhibit many of these features (Herring 1977; Holloway 1978; Zou & Holloway 1993).

The β-effect is not included in (1). This is in part because we shall examine approximate entropy calculation for isotropic turbulence below (cf. (3a)). Also, on doubly periodic β-plane one must calculate evolution of a spatially uniform flow $U(t)$ and decompose flow into $\psi - Uy$, leading to a self-consistent model describing evolution of ψ and U (see Hart (1979) for details). The canonical statistics for ψ are the same as (2) (Carnevale & Frederiksen 1987). Disequilibrium statistics are examined in Zou & Holloway (1993). In the present study we consider only f-plane dynamics for simplicity.

H theorems provide insight into the absolute equilibrium (2). The quantity that plays the central role is the entropy S, which measures the information necessary to specify the state of the fluid from only limited knowledge of quantities such as the second-order correlation matrix $\boldsymbol{Y}$. Maximizing S subject to the constraint given by knowledge

of $\boldsymbol{V}$ yields $S = \frac{1}{2}\ln\{\det \boldsymbol{V}\}$ (CFS). For the present problem, with statistical homogeneity of $\{\zeta_k\}$ and $\{h_k\}$,

$$S = \tfrac{1}{2}\sum_k \ln\{\langle\zeta_{-k}\zeta_k\rangle\langle h_{-k}h_k\rangle - |\langle\zeta_{-k}h_k\rangle|^2\}, \tag{3}$$

When only total energy and total enstrophy are known, the maximum of S (or minimum of information) constrained by $\langle E\rangle = E_0$ and $\langle Q\rangle = Q_0$ is obtained at $\langle\zeta_{-k}\zeta_k\rangle^{eq}$ and $\langle\zeta_{-k}h_k\rangle^{eq}$. Recent works by Miller (1990), Robert & Sommeria (1991), and Miller, Weichman & Cross (1992) emphasize the role of higher-order invariants of motion and show how to take them into account in a more general framework of equilibrium statistical mechanics. In the present study, we will choose initial conditions in an especially simple way such that information on higher-order invariants coincides with that preserved by truncated dynamics.

EDQNM closure equations of (1) imply

$$\mathrm{d}S/\mathrm{d}t = (\mathrm{d}S/\mathrm{d}t)_N + (\mathrm{dS}/\mathrm{d}t)_\nu, \tag{4}$$

where $(\mathrm{d}S/\mathrm{d}t)_N$ and $(\mathrm{d}S/\mathrm{d}t)_\nu$ symbolically represent the rates of entropy generation and dissipation, respectively. Nonlinear advection and topographic scattering contribute $(\mathrm{d}S/\mathrm{d}t)_N$. It is shown (CFS) that $(\mathrm{d}S/\mathrm{d}t)_N \geqslant 0$, with equality only at $\langle\zeta_{-k}\zeta_k\rangle^{eq}$ and $\langle\zeta_{-k}h_k\rangle^{eq}$. In the absence of dissipation, S monotonically increases to its maximum value. This, together with (2), suggests a correspondence between entropy maximization tendency and flow-topography correlation tendency in conservative systems.

In the presence of dissipation the correspondence is altered. Results depend on various factors including initial energy spectrum, the form and strength of dissipation. Nevertheless, nonlinear interaction and resulting entropy generation $(\mathrm{d}S/\mathrm{d}t)_N$ operate in dissipative systems as in conservative ones. For initial states far from absolute equilibrium, $(\mathrm{d}S/\mathrm{d}t)_N$ has been shown to dominate $(\mathrm{d}S/\mathrm{d}t)_\nu$ during the early phase of evolution (Carnevale 1982).

Some qualitative behaviours of S, which are found helpful in interpreting numerical results in the next section, may be observed from (4).

First, when ν_k is sufficiently small that local eddy turnover time $\tau_e(k) \equiv (k^3E(k))^{-\frac{1}{2}}$ is shorter compared with local viscous timescale $\tau_\nu(k) \equiv 1/\nu_k$ for all retained scales, approach to a quasi-equilibrium (or an instantaneous maximum entropy state) is expected (Fox & Orszag 1973). Moreover, since $(\mathrm{d}S/\mathrm{d}t)_N \simeq 0$ near instantaneous maximum entropy states, later evolution is characterized by entropy decay, with decay rate near the viscous decay rate,

$$\mathrm{d}S/\mathrm{d}t \simeq (\mathrm{d}S/\mathrm{d}t)_\nu = -\sum_k \nu_k.$$

Secondly, in the case of moderately to strongly scale-selective dissipation (e.g. $\nu_k \propto k^4$), $\tau_\nu(k)$ decreases quickly as $k \to k_{max}$, often resulting in $O[\tau_e(k)] \sim O[\tau_\nu(k)]$ for k near k_{max} and hence failure of relaxation at small scales. Approach to instantaneous maximum S states is not expected in the presence of such ν_k. Then $(\mathrm{d}S/\mathrm{d}t)_N$ does not approach zero but acts to compensate viscous loss of S. Hence, the actual decay rate of S is smaller than the viscous decay rate.

Thirdly, associated with scale-selective ν_k is selective decay of invariants of motion (Bretherton & Haidvogel 1976; Leith 1984). For system (1) Q decays relative to E (Bretherton & Haidvogel 1976). Minimizing Q subject to $E = E_0$ yields

$$\psi_k = h_k/(\gamma + k^2), \tag{5}$$

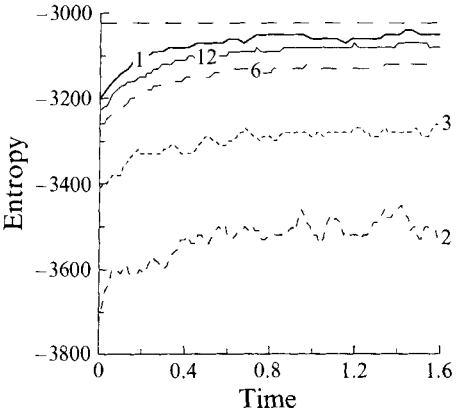

FIGURE 1. Entropy as a function of time. ——, Theoretical prediction of S from (2) and (3) using $\langle E \rangle$ and $\langle Q \rangle$ from 12-member ensemble runs. The thick line is for single realization using shell-averaging. Remaining curves correspond to 12, 6, 3, 2-member ensembles, respectively.

where γ is a Lagrange multiplier. Such minimum Q states are nonlinearly stable (Carnevale & Frederiksen 1987). Thus, in the case of scale-selective ν_k the system may seek a minimum enstrophy state while moving towards instantaneous maximum S under the action of $(\mathrm{d}S/\mathrm{d}t)_N$. The relevance of the two tendencies to the development of vorticity–topography correlation depends on the strength of scale-selective ν_k. For sufficiently weak ν_k, S maximization is expected to dominate, whereas for moderate to strong ν_k, Q minimization may act effectively after the initial stage of development.

3. Numerical results

The simulations presented below were conducted by integrating (1) in a circularly truncated spectral domain defined by $k \leqslant k_{max}$, with $k_{max} = 30$ unless stated otherwise, using the computer code in Zou & Holloway (1993). Time stepping is taken with leap-frog scheme, the triad summation calculated using spectral transformation (Orszag 1971), and dissipation treated analytically. The simulations start from initial fields generated according to energy spectrum

$$E(k) = e_0 k^2/(k_0^5 + k^5), \tag{6a}$$

or

$$E(k) = e_0 k^2 \exp(-(k/k_0)^2), \tag{6b}$$

with random phase. The topography h is set up from variance spectrum

$$H(k) = h_0/(3+k)^{2.5}. \tag{7}$$

Specifically, the amplitude of modal topography h_k is calculated according to $(H(k)/\pi k)^{\frac{1}{2}}$, with its phase uniformly distributed over $[0, 2\pi]$. By central limit theorem the topography thus constructed is approximately Gaussian. The constants e_0 and h_0 are chosen to give a prescribed ratio of r.m.s. vorticity ζ^0_{rms} to r.m.s. topography h_{rms}, where $\zeta^0_{rms} \equiv (\sum |\zeta_k|^2)^{\frac{1}{2}}$. The constant k_0 in (6) defines initial energy-containing scale.

The entropy expression (4) is undefined for wavenumber k where the argument of the logarithm vanishes. (The argument is non-negative by Schwarz inequality.) However, we ensured that this circumstance does not happen by assigning a topographic

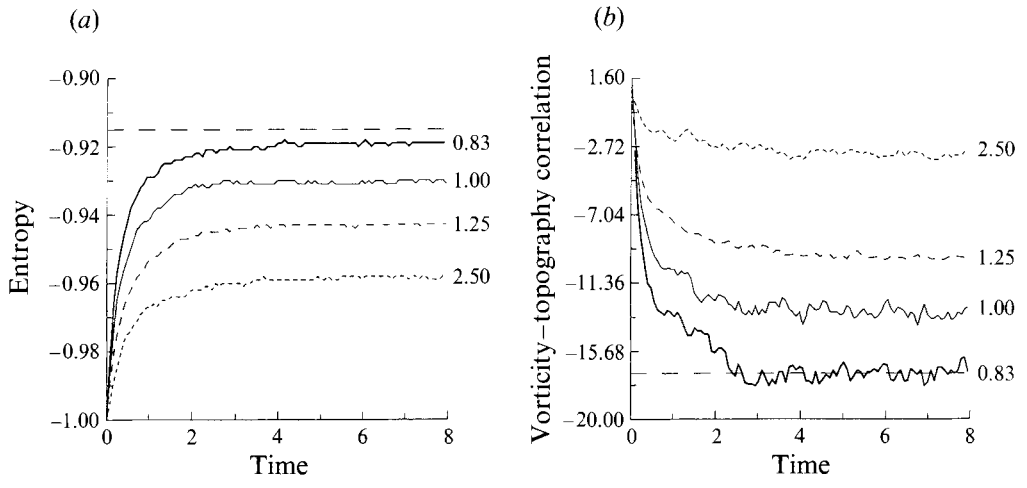

FIGURE 2. Inviscid cases. (*a*) Entropy and (*b*) vorticity–topography correlation. Horizontal dash lines are predicted by (2) and (3) for the case $\zeta^0_{rms}/h_{rms} = 0.83$. Remaining curves correspond to $\zeta^0_{rms}/h_{rms} = 0.83$, 1.00, 1.25 and 2.50, respectively. Time is expressed in terms of initial eddy turnover time $4\pi/\zeta^0_{rms}$, and entropy values have been normalized by their initial values.

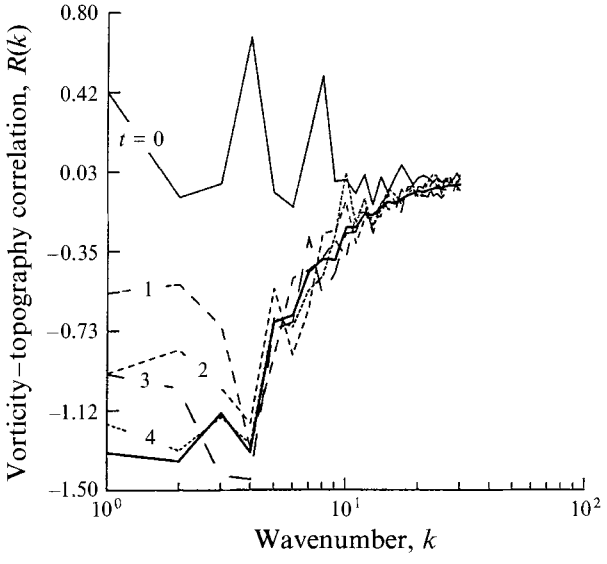

FIGURE 3. A sequence of vorticity–topography correlation spectra for the case $\zeta^0_{rms}/h_{rms} = 1.25$ in figure 2. The spectra correspond to $t = 0$, 1, 2, 3 and 4, respectively. The thick line is predicted by (2*c*).

spectrum and initializing the random vorticity field with non-vanishing variance at all k. During the period of decay of these finite experiments, vorticity variance did not fall below machine threshold at any k.

3.1. *Approximate entropy calculation for isotropic turbulence*

Evaluating S according to (3) requires an ensemble of realizations of (1). Acquiring a sufficient ensemble can be computationally demanding for long-time and high-

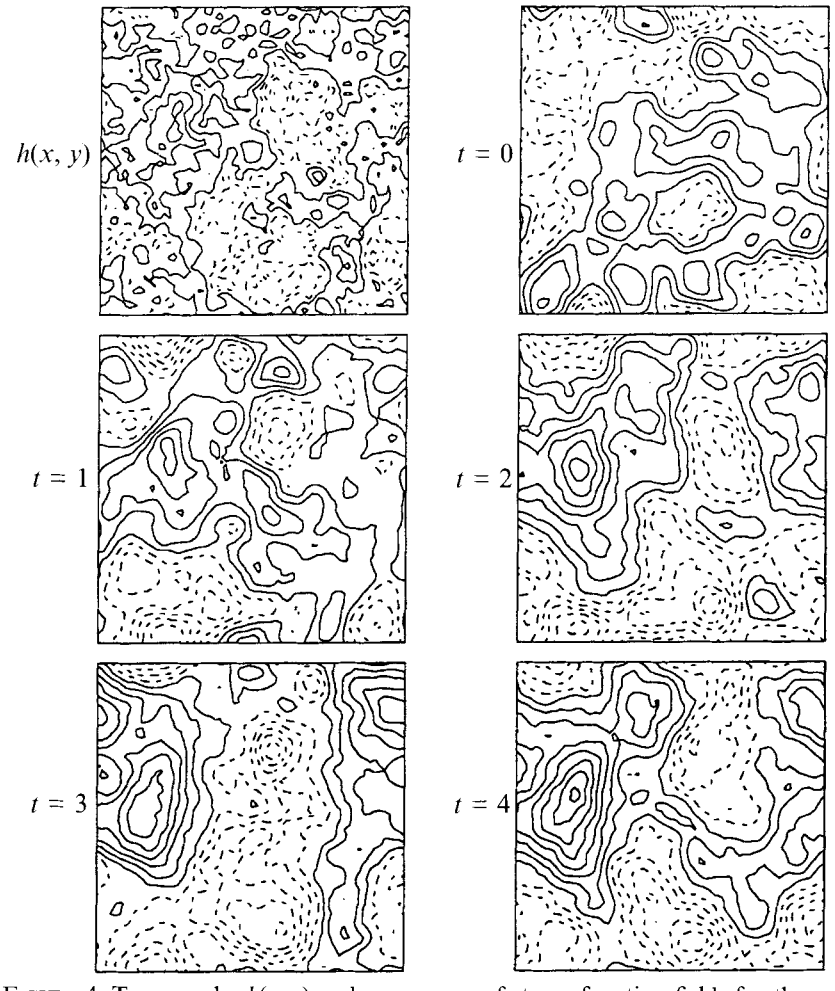

FIGURE 4. Topography $h(x, y)$ and a sequence of streamfunction fields for the same case as in figure 3.

resolution integrations. However, this may be avoided by approximating the ensemble average in (3) with shell average

$$\left.\begin{aligned} \langle \zeta_{-k}\zeta_k\rangle &\simeq Z(k)/2\pi k, \\ \langle h_{-k}h_k\rangle &\simeq H(k)/2\pi k, \\ |\langle \zeta_{-k}h_k\rangle|^2 &\simeq (R(k)/2\pi k)^2, \end{aligned}\right\} \tag{8}$$

where $$(Z(k), H(k), R(k)) \equiv \sum_{k-\frac{1}{2}<|k|<k+\frac{1}{2}} (|\zeta_k|^2, |h_k|^2, \mathrm{Re}\,(\zeta_{-k}h_k)).$$

This approximation is appropriate when the initial field $\{\zeta_k^0\}$ and topography $\{h_k\}$ are statistically isotropic, as in the present study.

A sequence of runs was made to test the approximation. Results are shown in figure 1. These runs are inviscid so that results can be compared with theoretically predicted values from (2) and (3). To explore the sensitivity of entropy to ensemble size the runs were also made with low resolution $k_{max} = 15$. Figure 1 shows S as a function of time. Also shown is the maximum entropy predicted by (2) and (3), with $\langle E\rangle$ and $\langle Q\rangle$ taken from the 12-member ensemble runs (cf. horizontal long-dash line). It is seen that a

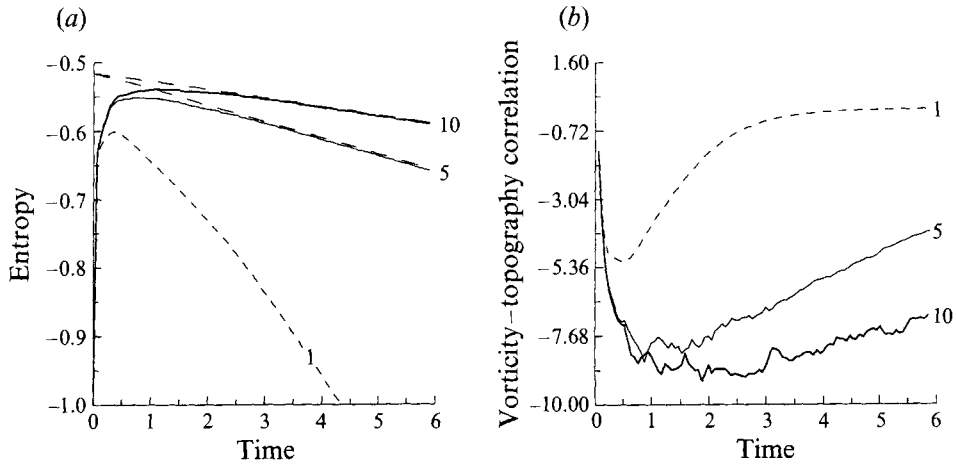

FIGURE 5. Rayleigh friction cases. (*a*) Entropy and (*b*) vorticity–topography correlation: ——, $\tau_\nu/\tau^0_{rms} = 10$; ——, = 5 and – – –, = 1. Curves — — in (*a*) are the instantaneous maximum S obtained from (2) and (3) using instantaneous E and Q for the case $\tau_\nu/\tau^0_{rms} = 10$ and 5, respectively.

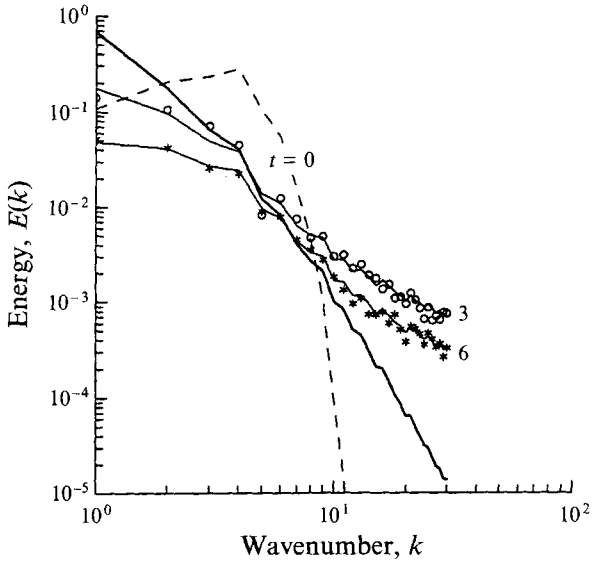

FIGURE 6. A sequence of energy spectra for the case $\tau_\nu/\tau^0_{rms} = 10$ in figure 5. $E(k)$ from the simulation: – – –, at $t = 0$; ○, at $t = 3$; *, at $t = 6$. ——, $E(k)$ for the instantaneous maximum S states at $t = 3$ and 6. ——, $E(k)$ for the minimum Q state (5).

small ensemble may result in underestimating entropy. Moreover, shell-averaged S is found insensitive to ensemble size. Therefore we adopted (8) for subsequent calculation of S.

3.2. *Results from inviscid runs*

Figures 2–4 give the results from inviscid simulations. These runs examine the correspondence between the entropy maximization tendency implied by the H theorem and development of vorticity–topography correlation suggested by the approach to (2). Figure 2(*a*) shows entropy time series from simulations. The initial fields and topography in these runs are set up according to (6*a*) with $k_0 = 4$ and (7), where e_0 and

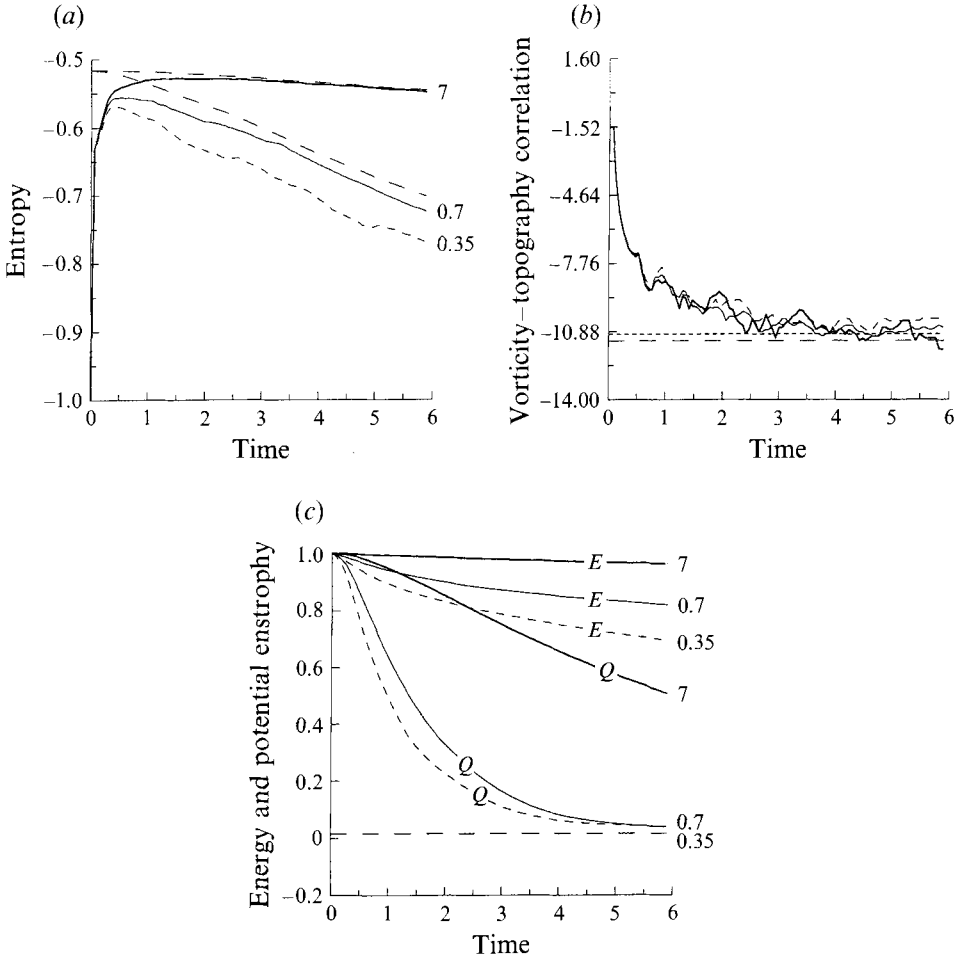

FIGURE 7. Laplacian friction cases. (*a*) Entropy, (*b*) vorticity–topography correlation and (*c*) energy and potential enstrophy. The thick solid, thin solid and shorter dash lines (——, $\tau_v/\tau^0_{rms} = 7$; ——, $= 0.7$; – – –, $= 0.35$. ——) in (*a*) are instantaneous maximum S for the case $\tau_v/\tau^0_{rms} = 7$ and 0.7. Curves —— and – – – in (*b*) are the correlations predicted respectively by the minimum Q state (5) with $\langle E\rangle = E_0 = 1$ and the maximum S state (2) with $\langle E\rangle = E_0 = 1$ and $\langle Q\rangle = Q_0 = 22.3$. Curve —— in (*c*) is the minimum Q from (5). For each pair of curves in (*c*), the upper one is for E and the lower for Q. S, E and Q are normalized by their initial values.

h_0 are chosen to give the ratio ζ^0_{rms}/h_{rms} ranging from 0.83 to 2.5. S exhibits rapid increases during an initial phase of evolution, followed by gradual transition to corresponding maxima with small fluctuations. Also shown in figure 2(*a*) is the maximum entropy predicted by the canonical statistics (2) and (3) for the case of $\zeta^0_{rms}/h_{rms} = 0.83$.

Note that S increases most rapidly during an initial eddy turnover time $\tau^0_{rms} \equiv 4\pi/\zeta^0_{rms}$. Figure 2(*b*) shows that this corresponds to the time over which vorticity–topography correlation develops. Figure 3 displays a sequence of correlation spectra $R(k)$ for the case of $\zeta^0_{rms}/h_{rms} = 1.25$. The initially rapid increase in S up to $t = 1.0$ (cf. figure 2*a*) reflects the onset of correlation at small to intermediate scales. Subsequent increase in S results from correlation development at large scales. Note that the faster approach to $\langle \zeta_{-k} h_k\rangle^{eq}$ at small scales than at large ones may be

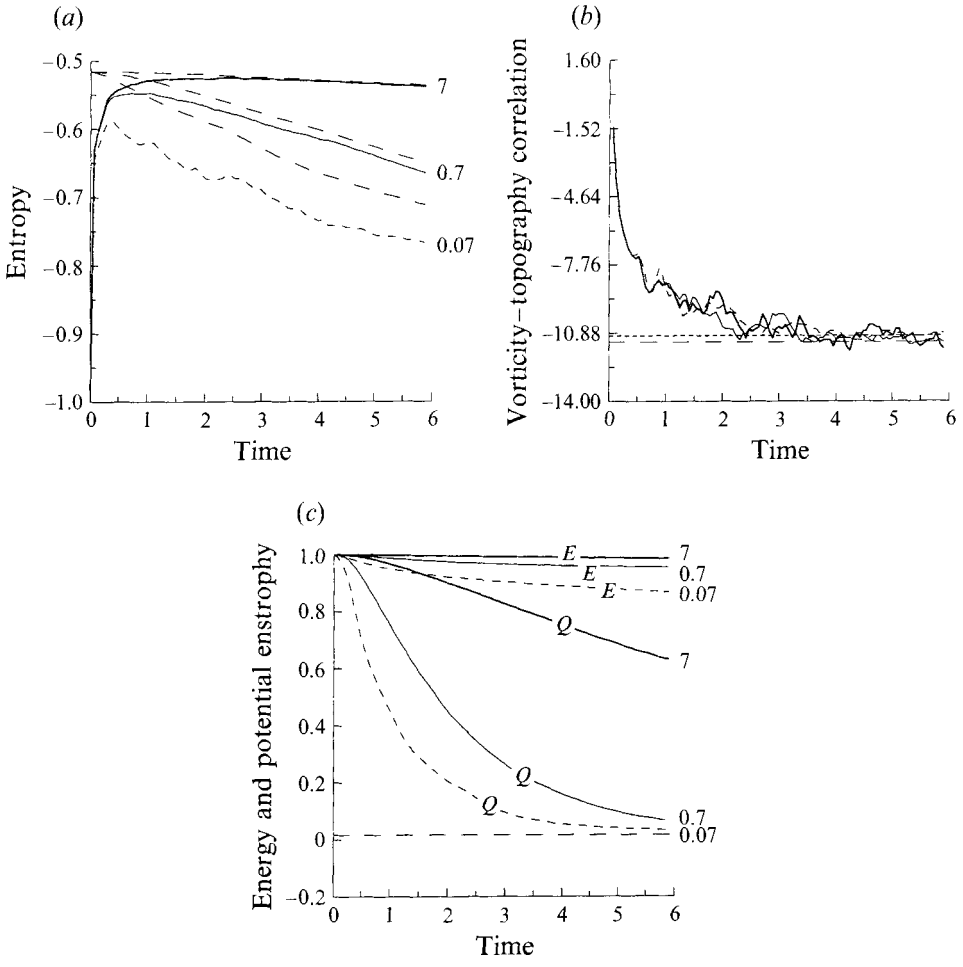

FIGURE 8. Biharmonic friction cases. (*a*) Entropy, (*b*) vorticity–topography correlation and (*c*) energy and potential enstrophy. ——, $\tau_\nu/\tau^0_{rms} = 7$; ——, $= 0.7$, – – –, $= 0.07$. The rest is as in figure 7.

anticipated from the shorter local eddy turnover time $\tau_e(k_{max}) = 0.3$ as compared with $\tau_e(k_{min}) = 7.4$. Evolution in physical space is shown in figure 4. By time $t = 4$ the flow is characterized on large scale by the anticyclonic circulations over 'bumps' and cyclonic circulation over 'dips'.

3.3. *Result from viscous runs*

Figures 5–9 show results from viscous runs, extending the correspondences seen in the inviscid cases to cases including dissipation. Three forms of dissipation are used, with different degrees of scale selectivity: (i) Rayleigh friction $\nu_k = \nu_0$, (ii) Laplacian friction $\nu_k = \nu_2 k^2$, and (iii) biharmonic friction $\nu_k = \nu_4 k^4$. The significance of viscous effects relative to inertia effects is measured by the ratio τ_ν/τ^0_{rms} evaluated at k_{max}, where $\tau_\nu \equiv 1/\nu_k$ is the local dissipation timescale. For each form of dissipation three runs are made corresponding to three values of this ratio, as summarized in table 1. The initial energy spectrum is given by (6*b*) with $k_0 = 4$, where e_0 is chosen, together with the choice of h_0 in (7), to give the ratio $\zeta^0_{rms}/h_{rms} = 1$. This form of initial energy spectrum is sufficiently away from the absolute equilibrium spectrum that $(\mathrm{d}S/\mathrm{d}t)_N$ is initially dominant in (4).

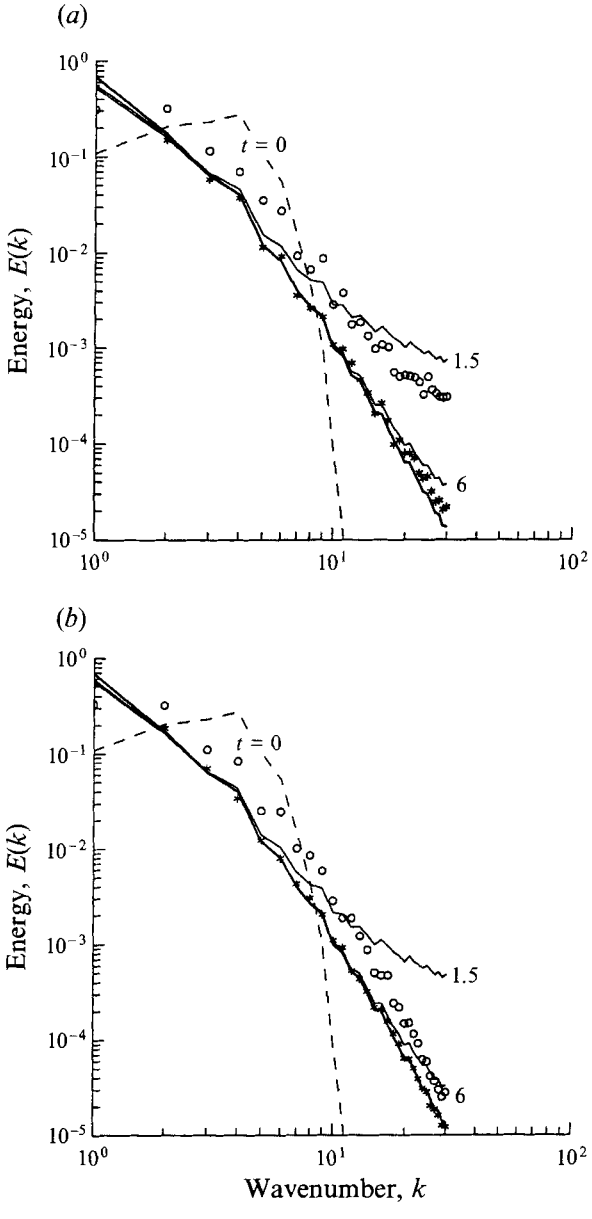

FIGURE 9. Sequence of energy spectra: (*a*) for the case $\tau_\nu/\tau^0_{rms} = 0.7$ in figure 7 and (*b*) for the case $\tau_\nu/\tau^0_{rms} = 0.07$ in figure 8. $E(k)$ from the simulation at: ---, $t = 0$; ○, $t = 1.5$; *, $t = 6$. ——, $E(k)$ for the instantaneous maximum S states at $t = 1.5$ and $t = 6$. ——, $E(k)$ for the minimum Q state (5).

Results for the Rayleigh friction cases (experiments 1–3) are given in figures 5 and 6. Entropy is shown in figure 5(*a*). Also shown are instantaneous maximum S for the cases of $\tau_\nu/\tau^0_{rms} = 5$ and 10, which are obtained from (2) and (3) using instantaneous E and Q. Entropy generation dominates the viscous dissipation initially, leading to rapid increases in S during the early phase of evolution. However, as the distance between actual states and instantaneous maximum S states decreases the entropy generation becomes weak and eventually is balanced by the dissipation. Subsequent evolution is characterized by entropy decay.

Exp	ν_0	ν_2	ν_4	τ_ν/τ^0_{rms}	$(\mathrm{d}S/\mathrm{d}t)_\nu$	$\overline{(\mathrm{d}S/\mathrm{d}t)}$
1	4.2×10^{-1}	—	—	1	−1243	−1219
2	8.4×10^{-2}	—	—	5	−246	−233
3	4.2×10^{-2}	—	—	10	−123	−120
4	—	9.4×10^{-4}	—	0.35	−1286	−365
5	—	4.7×10^{-4}	—	0.7	−643	−356
6	—	4.7×10^{-5}	—	7	−64	−58
7	—	—	5.2×10^{-6}	0.07	−4430	−271
8	—	—	5.2×10^{-7}	0.7	−443	−247
9	—	—	5.2×10^{-8}	7	−44	−38

TABLE 1. A list of viscous runs. ν_0, ν_2 and ν_4 are respectively the Rayleigh, Laplacian and biharmonic friction coefficients. τ_ν/τ^0_{rms} is the ratio, evaluated at k_{max}, of the local viscous timescale $\tau_\nu \equiv 1/\nu_k$ to the initial r.m.s. eddy turnover time ($\equiv 4\pi/\zeta^0_{rms}$), where ζ^0_{rms} is the initial r.m.s. vorticity. $(\mathrm{d}S/\mathrm{d}t)_\nu (= \Sigma_k \nu_k)$ is the entropy viscous decay rate implied by closure equations. $\overline{(\mathrm{d}S/\mathrm{d}t)}$ is the rate of entropy change in the simulations averaged over the later half simulation period.

Table 1 shows that actual decay rates for the three uniform damping runs are nearly the viscous decay rates, i.e.

$$\mathrm{d}S/\mathrm{d}t \simeq (\mathrm{d}S/\mathrm{d}t)_\nu = -\sum_k \nu_k.$$

This is expected from the earlier observation, that is, the approach to instantaneous maximum S states. The approach itself, say in the case of $\tau_\nu/\tau^0_{rms} = 10$, may be anticipated from the fact that $\tau_e(k) \leqslant \tau_e(1) = 2.3 \ll \tau_\nu(k) = 23$, at $t = 1.5$ and for all $k \leqslant k_{max}$. Figure 6 displays how the approach takes place in spectral space for the same case. By time $t \simeq 3$ the approach has been achieved at nearly all scales. In subsequent decay, actual energy spectra remain close to instantaneous maximum S states, implying $(\mathrm{d}S/\mathrm{d}t)_N \simeq 0$; hence the viscous decay rate approximates the actual decay rates. Note in figure 5(*a*) that the S increasing tendency prevails up to $t \leqslant 0.5$, 1.0 and 1.5 respectively for the three cases. Figure 5(*b*) shows that vorticity–topography correlation develops over these timescales.

Results from the scale-selective dissipation runs (experiments 4–9) are given in figures 7–9. Entropy maximization tendency proceeds initially much as before, but subsequent entropy decay depends on the strength of dissipation. For sufficiently weak ν_k the decay is similar to the previous cases, characterized by the approach to instantaneous maximum S states. Examples are the cases of $\tau_\nu/\tau^0_{rms} = 7$, shown by the thick solid lines in figures 7(*a*) and 8(*a*). Table 1 indicates that the actual decay rates for the two cases are near the viscous rates, as expected from the earlier observation about the small entropy generation rate $(\mathrm{d}S/\mathrm{d}t)_N$ near instantaneous maximum S states.

For the cases of moderate to strong dissipation, later evolution is characterized by (i) departure of actual S from instantaneous maximum S and (ii) actual decay rates smaller than viscous decay rates. Examples may be found in the cases $\tau_\nu/\tau^0_{rms} = 0.7$, shown by the thin solid lines in figures 7(*a*) and 8(*a*). This situation follows the observation about the failure of relaxation to instantaneous maximum S states at $k \to k_{max}$. One example is shown in figure 9(*a*). For $k \to k_{max}$ the actual energy spectra $E(k)$ depart from those of instantaneous maximum S states throughout the simulation. The departure induces $(\mathrm{d}S/\mathrm{d}t)_N$ which tends to compensate viscous loss of S, accounting for the departure in figure 7(*a*) and the smaller decay rate given in table 1. The departure in this case should be expected because $\tau_e(k) \to \tau_\nu(k)$ as $k \to k_{max}$.

More scale-selective ν_k leads to more pronounced departure at large k. The biharmonic friction case $\tau_\nu/\tau^0_{rms} = 0.7$ is shown in figure 9(*b*). The wider departure between the actual S and the instantaneous maximum S is shown in figure 8(*a*), with the larger difference between actual decay rate and viscous decay rate listed in table 1.

Comparison of the times on which S maximization proceeds (see figures 7(*a*) and 8(*a*)) with those for $\zeta-h$ correlation to develop (see figures 7(*b*) and 8(*b*)) shows that the two tendencies correspond well for sufficiently small dissipation. For strongly scale-selective damping the timescales of enstrophy minimization correspond more closely to the times for the correlation development (see figures 7(*c*) and 9(*c*)). Similar remarks hold for energy spectrum evolution. Specifically, experimental $E(k)$ can follow instantaneous maximum entropy energy spectrum (see figure 6), or minimum enstrophy energy spectrum (see figure 9*b*), or intermediate between the two (see figure 9*a*), depending on the extent of scale-selective dissipation. It should be pointed out that in the limit of infinite resolution the maximum entropy state has no fluctuating components and becomes identical to the minimum enstrophy state (Carnevale & Frederiksen 1987).

4. Discussion

The tendency for increasing entropy S has been examined in numerical simulation of turbulence over irregular topography. Results for conservative systems demonstrate correspondence between entropy maximization and the development of vorticity–topography correlation. When dissipation is included, S may increase initially and then decay. For cases with uniformly or weakly scale-selective damping, S approaches a quasi-equilibrium (maximum S subject to instantaneous, decaying energy and enstrophy). Further nonlinear generation of S is small, and S decays by explicit dissipation. For cases with strong, scale-selective damping, flows remain far from quasi-equilibrium. Onset of vorticity–topography correlation then corresponds to the timescale for selective decay of enstrophy relative to energy. Actual decay of S under strong, scale-selective damping results from a competition between nonlinear generation and loss to explicit damping.

We have made exploratory examination under special conditions. A host of further questions can and should be raised. We conclude with mention of some of these broader issues.

The topography used is statistically homogeneous. When a broad flat area is included in topography (such as an abyssal plane), eddy–topography interaction will proceed less effectively and the timescale for entropy maximization can be long (cf. Wang & Vallis 1993; Cummins & Holloway 1993). If the dissipation timescale is only a small fraction of the entropy maximization timescale, eddies initially released over flat areas may be dissipated before the maximum entropy state is realized.

The formulation adopted here is based on energy and enstrophy ensemble. These are the only invariants (other than circulation and linear momentum) preserved by the spectrally truncated system such as (1) despite the fact that the corresponding continuum system also has higher-order vorticity invariants. The presumption underlying the energy–enstrophy ensemble approach (Kraichnan 1975) is that the hypersurfaces of higher-order invariants sample the surface of constant energy and enstrophy so frequently that statistics of ensemble realizations of turbulence can be determined from averaging over the energy–enstrophy ensemble. There have been evidences in support of the energy–enstrophy based theories, among which is the robust approach to the absolute equilibrium from a random initial field (Fox & Orszag

1973; Basdevant & Sadourny 1975; Kells & Orszag 1978; Carnevale 1982; Kaneda, Gotoh & Bekki 1989).

Possible existence of nonlinear stable states (Carnevale & Frederiksen 1987; Shepherd 1987) are at variance with the energy–enstrophy based theories. As shown in Shepherd (1987), for sufficiently large value of β, there may exist a subset of finite measure on the energy–enstrophy ensemble which does not effectively mix with hypersurfaces of higher-order invariants. Recent efforts by Miller (1990), Robert & Sommeria (1991), and Miller *et al.* (1992) show how the higher-order invariants can be taken into account in determining statistical equilibrium states.

In the present study we have strived to set up the experiments as simply as possible while retaining essential dynamics for exploring the entropy maximization and enstrophy minimization in the same context. We have omitted β. More importantly, we have constructed the initial conditions from (6) with random phase, which approach joint-Gaussianity by the central limit theorem. This simple design has the consequence that the higher-order invariants are fully implied by moments up to second order. This condition for the higher-order invariants would be preserved by inviscid dynamics coincidentally with the tendency we actually compute from truncated spectral dynamics.

We thank Professor Y. Kaneda, Drs B. Tang and P. F. Cummins for interesting discussions. This research has been supported by the Office of Naval Research (N00014-87-J-1262).

REFERENCES

BASDEVANT, C. & SADOURNY, R. 1975 Ergodic properties of inviscid truncated models of two-dimensional incompressible flows. *J. Fluid Mech.* **69**, 673–688.

BRETHERTON, F. P. & HAIDVOGEL, D. B. 1976 Two-dimensional turbulence above topography. *J. Fluid Mech.* **78**, 129–154.

CARNEVALE, G. F. 1982 Statistical features of the evolution of two-dimensional turbulence. *J. Fluid Mech.* **122**, 143–153.

CARNEVALE, G. F. & FREDERIKSEN, J. S. 1987 Nonlinear stability and statistical mechanics of flow over topography. *J. Fluid Mech.* **175**, 157–181.

CARNEVALE, G. F., FRISCH, U. & SALMON, R. 1981 *H* theorems in statistical fluid dynamics. *J. Phys.* A: *Math. Gen.* **14**, 1701–1718.

CARNEVALE, G. F. & HOLLOWAY, G. 1982 Information decay and predictability of turbulent flows. *J. Fluid Mech.* **116**, 115–121.

CARNEVALE, G. F. & VALLIS, G. K. 1984 Applications of entropy to predictability theory. In *Predictability of Fluid Motions*, ed. G. Holloway & B. J. West, pp. 577–592. New York: Am. Inst. Phys.

CUMMINS, P. F. 1992 Inertial gyres in decaying and forced geostrophic turbulence. *J. Mar. Res.* **50**, 545–566.

CUMMINS, P. F. & HOLLOWAY, G. 1994 On eddy-topographic stress representation. *J. Phys. Oceangr.* (in press).

FOX, D. G. & ORSZAG, S. A. 1973 Inviscid dynamics of two-dimensional turbulence. *Phys. Fluids* **16**, 169–171.

GRIFFA, A. & SALMON, R. 1989 Wind-driven ocean circulation and equilibrium statistical mechanics. *J. Mar. Res.* **47**, 457–492.

FREDERIKSEN, J. S. & BELL, R. C. 1983 Statistical dynamics of internal gravity waves-turbulence. *Geophys. Astrophys. Fluid Dyn.* **26**, 257–301.

FREDERIKSEN, J. S. & BELL, R. C. 1984 Energy and entropy evolution of interacting internal gravity waves and turbulence. *Geophys. Astrophys. Fluid Dyn.* **28**, 171–203.

FREDERIKSEN, J. S. & SAWFORD, B. L. 1980 Statistical dynamics of two-dimensional inviscid flow on a sphere. *J. Atmos. Sci.* **37**, 717–732.

HART, J. E. 1979 Barotropic quasi-geostrophic flow over anisotropic mountains. *J. Atmos. Sci.* **36**, 1736–1746.

HERRING, J. R. 1977 On the statistical theory of two-dimensional topographic turbulence. *J. Atmos. Sci.* **34**, 1731–1750.

HOLLOWAY, G. 1978 A spectral theory of nonlinear barotropic motion above irregular topography. *J. Phys. Oceangr.* **8**, 414–427.

HOLLOWAY, G. 1986 Comment on Fofonoff's mode. *Geophys. Astrophys. Fluid Dyn.* **37**, 165–169.

HOLLOWAY, G. 1992 Representing topographic stress in large scale ocean models. *J. Phys. Oceangr.* **22**, 1033–1046.

KANEDA, Y., GOTOH, T. & BEKKI, N. 1989 Dynamics of inviscid truncated model of two-dimensional turbulence shear flow. *Phys. Fluid* **1** (7), 1225–1234.

KELLS, L. C. & ORSZAG, S. A. 1978 Randomness of low-order models of two-dimensional inviscid dynamics. *Phys. Fluids* **21**, 162–168.

KRAICHNAN, R. H. 1975 Statistical dynamics of two-dimensional flow. *J. Fluid Mech.* **67**, 155–175.

LEITH, C. E. 1984 Minimum enstrophy vortices. *Phys. Fluids* **27**, 1388–1395.

MILLER, J. 1990 Statistical mechanics of Euler equation in two-dimensions. *Phys. Rev. Lett.* **65**, 2137–2140.

MILLER, J., WEICHMAN, P. B. & CROSS, M. C. 1992 Statistical mechanics, Euler's equation and Jupiter's red spot. *Phys. Rev.* A **45**, 2328–2359.

ORSZAG, S. A. 1971 Numerical simulation of incompressible flows with simple boundaries. I. Galerkin (spectral) representation. *Stud. in Appl. Maths* **4**, 293–327.

ROBERT, R. & SOMMERIA, J. 1991 Statistical equilibrium states for two-dimensional flows. *J. Fluid Mech.* **229**, 291–310.

SALMON, R., HOLLOWAY, G. & HENDERSHOTT, M. C. 1976 The equilibrium statistical mechanics of simple quasi-geostrophic models. *J. Fluid Mech.* **75**, 691–703.

SHEPHERD, T. G. 1987 Non-ergodicity of inviscid two-dimensional flow on a beta-plane and on the surface of a rotating sphere. *J. Fluid Mech.* **184**, 289–302.

WANG, J. & VALLIS, G. 1993 Emergence of Fofonoff states in inviscid and viscous ocean circulation models. *J. Mar. Res.* (in press).

ZOU, J. & HOLLOWAY, G. 1993 Forced-dissipated statistical equilibrium of large scale quasi-geostrophic flows over random topography. *Geophys. Astrophys. Fluid Dyn.* **69**, 55–75.